REGIONAL LOCATION AND IDENTIFICATION USING SPARSE STATIONS

Brian Savage, Ying Tan, Lupei Zhu, and Don Helmberger

California Institute of Technology, Seismological Laboratory

Sponsored by Defense Threat Reduction Agency

Contract No. DSWA01-98-0010

ABSTRACT

Locating events in Southern California is quite simple since we have about 500 stations, with a large fraction broadband (TriNet). We locate and identify within minutes. Thus, we have an opportunity to test hybrid methods against the full array estimate. Here we report on three projects addressing these issues; (1) locating events using one calibrated station with waveform data plus a few other stations with travel-time and polarity information, (2) particularly complex sub-regions where the depth phases such as pPn and sPn prove ineffective, and (3) calibrating paths using a combination of sparse regional waveforms and radar.

In previous efforts (last years report) we presented results using waveforms from one-station (PAS) and a few polarities from the array (3 to 5). The model employed a grid-search over mechanism (strike, dip and rake) with the depth fixed. Along most paths the method proved effective when comparing against the entire network. Here we present results of letting the depth vary as well so that the single station must use pPn and sPn and the ratio of body waves to surface waves to fix the depth. Only about half the paths still work, but in those situations, the location is greatly improved over just travel-time fitting because of the whole seismogram matching procedure. Our method uses an adaptive grid search over location with calibrated Pnl and surface wave time shifts.

However, the corrections to 1-D models are only applicable to areas in which the velocity structure does not vary drastically. Refracted phases, like Pn, at distances over 200 km provide most P arrival times. When the velocity structure begins to vary drastically near the source, the receiver, or along the propagation path, the arrival times vary greatly. Moreover, the structure modifies the waveform shape such that it makes identification of Pn and its associated depth phases exceedingly difficult. Such an area occurs beneath the high Southern Sierras through Owens Valley and into Death Valley. A low velocity zone, relative to the mantle, exists directly under the Moho and creates extra arrivals. These extra arrivals could be misconstrued as depth phases and thus a mis-location. Steps to identify areas of dramatic velocity variation, such as the one noted previously or in and around the Tibetian plateau, are needed to avoid misinterpretation of direct arrivals and depth phases.

In lieu of robust event locations, regional path calibration and crustal modeling utilizes well-located explosions, such as seismic reflection/refraction experiments or isolated blasts [Kanamori and Hadley (1975)]. In regions that include no well-located seismic events, other methods of path calibration are needed. Using InSAR (Interferometric Synthetic Aperture Radar) data to locate earthquakes provides the necessary ground truth to accomplish regional path calibration, leading to more accurate event locations. By using InSAR data to constrain the location and seismic data to determine the mechanism, the combination characterizes events robustly. As shown by Lohman et al. (2001) for the 1992 Little Skull Mountain event, InSAR data has the ability to locate events to within 0.5 km in the horizontal direction and 1.0 km in the vertical. Even with limited data coverage, this approach provides excellent constraints on location and mechanism, natural or man-made. Corrections to simple 1-D models can be made by using locations derived from InSAR data. These corrections are then used to locate events in an accurate fashion.

KEY WORDS: location, regional model calibration, InSAR, seismic, complex sub regions

OBJECTIVE

The objective of this study is to develop new and improve on existing techniques of locating events, in depth and surface expression. Several problems have been identified with the event location process, such as the trade-off between depth and origin time and the lack of high quailty data due to sparseness of regional seismic networks, which are usually short-period vertical seismometers. Development of new methods within Southern California to coincide with sparse station distribution provides error estimates associated with new methods and ways to reduce these errors. In conjunction, use of ground-truth events to calibrate regional paths, we may readily identify areas of three dimensional structure to accurately locate events further.

RESEARCH ACCOMPLISHED

Issues involving one-station solutions were covered at a recent DTRA workshop (Kansas City, 2001) and will be omitted in this report where we will concentrate on the detailed Pnl wavetrain (Pn, pPn, and sPn). However, we will also address the merits of using both radar (static field) and the seismic-wavefield (dynamic) together to study earthquakes.

Pn Complexity

Through the use of three large events in central California we are able to illuminate areas of regional seismic wave propagation, the crust and upper mantle, to determine appropriate corrections to 1-D models and begin to develop 3-D models.

Data from an event in Santa Rosa, CA is shown, but not modeled as a profile, as it is does not provide a simple 2-D profile due to large azimuth swings. Selected waveform data is shown in figure 1b and time picks from the stations within California are shown as a map in figure 1a. As the arrivals approach the Sierras and the Basin and Range, Pn delays grow larger and then reach a maximum at Mammoth, CA. About 1 second of this delay at Mammoth is a result of local structure. Stations further to the southeast also show late Pn arrivals. The Pn arrivals in the northern portion are longer period than the faster Pn arrivals to the south, suggesting complex structure. The data suggests a very sharp boundary between KCC and MLAC and a gradual increase in velocity, greater than 8.0 km/sec, further to the southeast. As the data suggests and as is also seen by Pn tomography, a slow velocity anomaly appears underneath the Sierra Nevada and areas to the east.

A second event in Mammoth, CA and the locale of TriNet in southern California allows the creation of a record section down the axis of the southern Sierra Nevada. Figure 2 shows stations used for this profile in blue, while figure 3 displays the velocity data. The radial, not shown, and vertical components are similar in nature, indicating little anomalous structure near the receivers. A 1-D record section, shown for reference, incorporates a mantle velocity of 8.0 km/sec and a simple crust of 6.3 km/sec in figure 4. The arrivals in figure 4 are refractions, as they are single sided pulses in velocity, while reflections are double sided. The two single sided pulses are Pn and sPn, with Pn arriving first, as sPn must travel to the surface as an S-wave, then traverse much the same path as Pn. Arrivals propagating down the southern Sierra Nevada axis include an anomalous second arrival with a large downswing following the initial Pn, figure 3. This is either a set of two refractions, with opposite amplitudes, or a reflection off a boundary near the Moho. The arrival is consistently behind Pn by 0.75-1.0 seconds, indicating it travels at the same speed and through the same material.

By adding a slow region on the source side, as shown in figure 5, a second arrival appears behind Pn with the timing adjusted by the velocity and the depth extent of the anomaly, figure 3. We add the anomaly on the source side because the secondary arrival exists across the entire section of data. The velocity of 7.6 km/sec is similar to that seen by (Zhao, 93) and (Carder, 1973). The second arrival is a reflection off the bottom of this feature. At distances over 350 km the reflection travels in the mantle just below the Moho, similar to a refraction in speed but double-sided in shape. At distances less than 350 km the second arrival diverges from Pn as it must travel to the base and back entirely within the anomaly. If the bottom of the

anomaly dips away from the source, figure 5, then the timing of the second arrival, at shorter distances, decreases relative to Pn as it travels a smaller distance than before, as shown in figure 3.

In this section we analyze what a crustal root does to seismograms as they travel down the axis of a mountain chain, in the same orientation as the previous profile. Three models with varying crustal roots are approximations of those in (Pakiser and Brune, 1980). Each crustal root model shows two distinct arrivals independent of the crustal thickness, figure 6. However, the depth of the crustal root directly affects the absolute timing of Pn, pPn, and sPn. Examining the records past the first arrival, the main difference between the crustal and mantle root models is the presence of the large downswing in the mantle anomaly models. Data traveling down the Sierran axis also shows this downswing, giving more credence to the anomalous mantle rather than crustal root model.

Utilizing a third event in Nevada, we produce a profile along Death Valley's eastern edge with station in the red profile in figure 2 and the velocity data in figure 7. Comparing this velocity data with synthetics for the 1-D model in figure 4, the similarities and simplicity in the seismic waveforms at distances up to 600 km appear. For this reason, we interpret the eastern section of data propagating down Death Valley and the California-Nevada border as 1-D. The travel times of Pn and sPn increases as the distance increases relative to a 8.0 km/sec mantle, but the simplicity of the data does not warrant extra structure, only small velocity shifts along the propagation path. Model Eastern Mojave, figure 8, created specifically for this data set, adds additional layers to a layer over a half-space, and accurately predicts the data, figure 7. Addition of the tectonic North America (TNA) (Grand and Helmberger, 1984) mantle, for completeness, adds nothing to the waveforms at these distances for the types of arrivals we consider.

Regional seismic data, through the use of Pnl waveforms, has efficiently identified distinct and separate provinces. A region of one-dimensional structure exists on the border between California and Nevada extending through the crust into the mantle, the area where first-arriving regional travel. A second distinct region to the west beneath the southern Sierra Nevada Mountains exists only within the mantle. The mantle has a velocity of 7.6 km/sec, different than the 7.8-8.0 km/sec normally seen. The anomaly extends down to depths of 75-100 km.

InSAR Locations

InSAR data alone and a combination of InSAR and regional seismic data to locate and determine the source parameters of events was tested for the well-studied 1992 Little Skull Mountain earthquake. We invert using a non-linear technique, the Neighborhood Algorithm, to solve for the location, source, slip and area. Figure 9 shows the Little Skull Mountain earthquake InSAR scene with solutions from previous investigators.

For the InSAR-only inversion we find a large tradeoff between slip and area, figure 10a, whereas the seismic moment is well constrained to be about $4.4 * 10^{17}$Nm (Mw 5.7), figure 10b. Since the area is not well constrained by our data, we adopt a value of 25 km^2 as estimated from aftershock distributions (Harmsen, 1994; Meremonte et al., 1995; Smith et al., 2000) and that is used in previous studies (Wernicke et al., 1998; Savage et al., 1999).

When we invert using only the InSAR data, and assume a fixed fault area of 25 km^2, a search through the entire range of potential mechanisms suggests a best fitting mechanism with a rake of 47^o. This estimate of the rake is much shallower than predictions from previous seismic studies. Figure 10c shows the map view locations of best-fitting fault planes of area 25 km^2 from inversions where we fixed the rake at values between -20^o and -100^o. All of these models have similar misfits to the InSAR data, illustrating the tradeoff between earthquake mechanism and location inherent with this set of InSAR data. If additional InSAR data existed with a different LOS direction, we would be better able to determine the mechanism and thus the location.

Since additional InSAR data is not available we turn to seismic data to tightly constrain the mechanism of the LSM earthquake. However the seismic data contains relatively little information on the location, as accurate as InSAR would procvide. Both layered models, Standard Southern California and Mojave,

predict mechanisms and moments that are well within the range of predictions from previous seismic studies. Both of these mechanisms fit the seismic data very well, but do not fit the InSAR data well.

Our initial attempt at a simultaneous joint inversion calculates misfits to both the seismic and InSAR data, weighted by the RMS value of each data set. This inversion approach results in models that average the parameters from the InSAR-only and seismic-only inversions and fit neither data set well. Using the InSAR data to relocate the best-fitting mechanism inferred from only the seismic data produces a better result. We iterate between seismic-only and InSAR-only inversions multiple times. Figure 11 shows the mechanism for the Mojave elastic model and the associated misfits. This result fits both the seismic and the InSAR data well. Synthetic waveforms calculated from the best-fitting mechanism from the inversion using only InSAR data do not fit the seismic data nearly as well as does the one from the joint inversion figure 11. The joint InSAR/seismic inversion produces a mechanism that is 1km shallower than the InSAR-only inversion and predicts a moment of $4.1*10^{17}$Nm (Mw 5.7).

InSAR data can effectively locate shallow earthquakes that are too small or too distant to accurately locate using traditional seismic methods. In this study, the InSAR data is sensitive to the seismic moment of the earthquake, but suffers from a tradeoff between mechanism and location. The seismic data is sensitive to the mechanism, but not to the location. Both data types are unable to separate area from magnitude of slip, or to distinguish which of the two potential conjugate planes ruptured. The main observational limitations of this study are the availability of only one SAR image before the earthquake and the existence of only one component of deformation.

CONCLUSIONS AND RECOMMENDATIONS

A large anomaly of slow mantle velocity appears underneath the Sierras and the valleys to the east. While, a crustal root is not possible when examining the Mammoth earthquake profile down the Sierra Nevada axis. Results of this type compare well with those of Savage et al. (1994), Carder et al.(1970), and Carder (1973). The lack of a high velocity lid could explain the data shown by Melbourne (2000) and the tomography of Zhao (1993). There also appears to be a large velocity contrast at about 75-100 km depth below the eastern California shear zone. Identification of anomalies such as this are useful, in that they may be accounted for in terms of the first arriving Pn travel times. Future investigations may be accomplished using Pn tomography and simple waveform analysis.

Hopefully, future studies of small events will have more independent interferograms and therefore will permit greater averaging to reduce noise. We must also be able to measure multiple components of the deformation in order to improve the ability of InSAR data to determine earthquake mechanisms. Beyond the discussion of the LSM earthquake, this study supports the feasibility of the formation of a catalogue of earthquakes located using both InSAR and seismic data. This catalogue could support regional path calibration which can benefit from improved bounds on source locations. In many regions of the world earthquake location error is greater than 25 km. For many of these events this uncertainty can be reduced by two orders of magnitude.

REFERENCES

Bolt, B.A. and R. Gutdeutsch, Reinterpretation by ray tracing of a Transverse Refraction Seismic Profile through the California Sierra Nevada, Part 1, *Bull. Seismo. Soc. Am.*, 72, 3, 889-900, 1982

Byerly, P, Comment on "The Sierra Nevada in the Light of Isostasy", *Bull. Geol. Soc. Am.*, 2025-2031, 1937

Carder, D.S. and A. Qamar and T.V. McEvilly, Trans-California Seismic Profile-Pahute Mesa to San Francisco Bay, *Bull. Seismo. Soc. Am.*, 60, 6, 1829-1846, 1970

Carder, D.S, Trans-California Seismic Profile, Death Valley to Monterey Bay, *Bull. Seismo. Soc. Am.*, 63, 2, 571-586, 1973

Eaton, J.P., Crustal structure in northern and central California from seismic evidence, *Bull. Cal. Div. Mines. Geol*., 190, 419-426, 1966

Fliedner, M.M. and S. Ruppert, Three-dimensional crustal structure of the southern Sierra Nvada from seismic fan profiles and gravity modeling, *Geology*, 24, 4, 367-370, 1996

Grand, S.P. and D.V. Helmberger, Upper mantle shear structure of North America, *Geophys. J. Roy. Astr. S.* , 76, 399-348, 1984

Hadley, D. and H. Kanamori, Seismic structure of the Transverse Ranges, California, *Geol. Soc. Am. Bull*., 88, 1469-1478, 1977

Harmsen, S. C., The Little Skull Mountain, Nevada, Earthquake of 29 June 1992: Aftershock Focal Mechanisms and Tectonic Stress Field Implications, *Bull. Seismo. Soc. Am*., 84, 1484-1505, 1994

Helmberger D.V. and G.R. Engen, Modeling the Long-Period Body Waves from Shallow Earthquakes at Regional Ranges, *Bull. Seismo. Soc. Am*., 70, 5, 1699-1714, 1980

Helmberger, D.V. and J.E. Vidale, Modeling Strong Motions produced by Earthquakes with Two-Dimensional Numerical Codes, *Bull. Seismo. Soc. Am*., 78, 1, 109-121, 1988

Jones, C.H., Is Extension in Death Valley Accommodated by Thinning of the Mantle Lithosphere beneath the Sierra Nevada, California, *Tectonics*, 6, 4, 449-473, 1987

Jones C.H. and H. Kanamori and S. W. Roecker, Missing roots and Mantle "drips": Regional Pn and teleseismic arrival times in the southern Sierra Nevada and vicinity, California, *Jour. Geophys. Res.*, 99, B3, 4567-4601, 1994

Jones, C.H. and R.A. Phinney, Seismic structure of the lithosphere from teleseismic converted arrivals observed at small arrays in the southern Sierra Nevada and vicinity, California, *Jour. Geophys. Res.*, 103, B5, 10,065-10,090, 1998

Jones, L. E. and D. V. Helmberger, Earthquake source parameters and fault kinetics in the eastern California shear zone, *Bull. Seismo. Soc. Am*., 88, 1337-1352, 1998

Lawson, A.C., The Sierra Nevada in the Light of Isostasy, *Bull. Geol. Soc. Am*., 47, 1691-1712, 1936

Melbourne, T. and D. Helmberger, Mantle Control of the Plate Boundary Deformation?, In perpetration, 2000

Massonnet, D., and K. L. Feigl, Radar interferometry and its application to changes in the earth's surface, *Rev. Geophys*., 36, 441-500, 1998

Meremonte, M., J. Gomberg, and E. Cranswick, Constraints on the 29 June 1992 Little Skull Mountain, Nevada, Earthquake Sequence Provided by Robust Hypocenter Estimates*, Bull. Seismo. Soc. Am.*, 85, 1039-1049, 1995

Okada, Y., Surface deformation due to shear and tensile faults in a half space, *Bull. Seismo. Soc. Am*., 75, 1135-1154, 1985

Pakiser, L.C. and J.N. Brune, Seismic Models of the Root of the Sierra Nevada, *Science*, 210, 5, 1088-1094, 1980

Romanowicz, B., D. Dreger, M. Pasyanos, and R. Uhrhammer, Monitoring of Strain Release in Central and Northern California using Broadband Data, *Geophys. Res. Lett*., 20, 1643-1646, 1993

Rosen, P. A., S. Hensley, I. R. Joughin, F. K. Li, S. N. Madsen, E. Rodriguez, and R. M. Goldstein, Synthetic Aperture Radar Interferometry, *Proc. of the IEEE*, 88, 333-382, 2000

Sambridge, M., Geophysical inversion with a neighborhood algorithm - I, Searching a parameter space, *Geophys. Jour. Int*., 138, 479-494, 1998

Sambridge, M., Geophysical inversion with a neighborhood algorithm - II, Appraising the ensemble, *Geophys. Jour. Int*. 138, 727-746, 1998

Savage, B. and D.V. Helmberger, The Sinking of the Kursk, *Bull. Seismo. Soc. Am*., In press, 2001

Savage, J. C., M. Lisowski, W. K. Gross, N. E. King, and J. L. Svarc, Strain accumulation near Yucca Mountain, Nevada, 1983-1993, *Jour. Geophys. Res*., 99, 18103-18107, 1994

Savage, J. C., J. L. Svarc, and W. H. Prescott, Strain accumulation at Yucca Mountain, Nevada, 1983-1998, *Jour. Geophys. Res*.,104, 17627-17631, 1999

Savage, M.K. and L. Li and J.P. Eaton and C.H. Jones and J.N. Brune, Earthquake refraction profiles of the root of the Sierra Nevada, *Tectonics*, 13, 4, 803-817, 1994

Simons, M. and Y. Fialko, On the efficient use of continuous geodetic imagery, in preparation, 2001

Smith, K. D., J. N. Brune, D. dePolo, M. K. Savage, R. Anooshehpoor, and A. F. Sheehan, The 1992 Little Skull Mountain Earthquake Sequence, Southern Nevada Test Site", U. S. Geol. Surv. Digital Data Series DDS-058, Chapter K, 1-16, 2000

Walter, W., Source Parameters of the June 29, 1992 Little Skull Mountain Earthquake from Complete Regional Waveforms at a Single Station, *Geophys. Res. Lett*. , 20, 403-406, 1993

Wang, C. Y. and R. B. Herrmann, A numerical study of P, SV, and SH-wave generation in a plane layered medium, *Bull. Seismo. Soc. Am*., 70, 1015-1036, 1980

Wernicke, B.and R. Clayton and M. Ducea and C.H. Jones and S. Park and S. Ruppert and J. Saleeby and J. K. Snow and L. Squires and M. Fliedner and G. Jiracek and R. Keller and S. Klemperer and J. Luetgert and P. Malin and K. Miller and W. Mooney and H. Oliver and R. Phinney, Origin of high mountains in the continents: The southern Sierra Nevada, *Science*, 271, 5246, 190-193, 1996

Wernicke, B., J. L. Davis, R. A. Bennett, P. Elosegui, M. J. Abolins, R. J. Brady, M. A. House, N. A. Niemi, and J. K. Snow, Anomalous Strain Accumulation in the Yucca Mountain Area, Nevada, *Science*, 279, 2096-2100, 1998

Zhao, L.S., Lateral Variations and Azimuthal Isotropy on Pn Velocities Beneath Basin and Range Province, *Jour. Geophys. Res*., 98, B12, 22,109-22,122, 1993

Zhao, L. and D. V. Helmberger, Source Estimation from Broadband Regional Seismograms, *Bull. Seismo. Soc. Am*., 84, 91-104, 1994

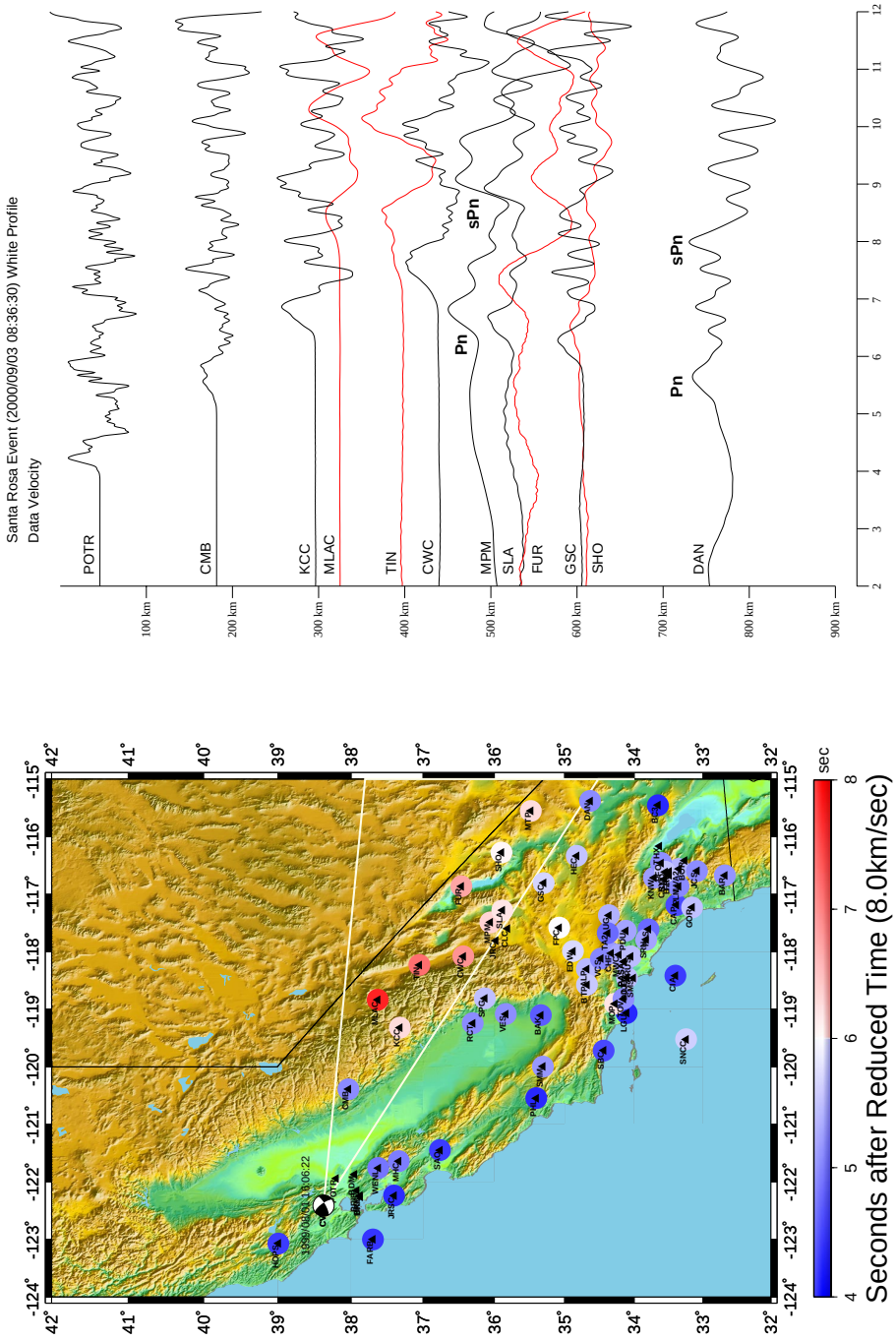

Figure 1. a) Pn time picks where the color is the delay after an arrival of 8.0 km/sec. b)Velocity data from Santa Rosa Earthquake.

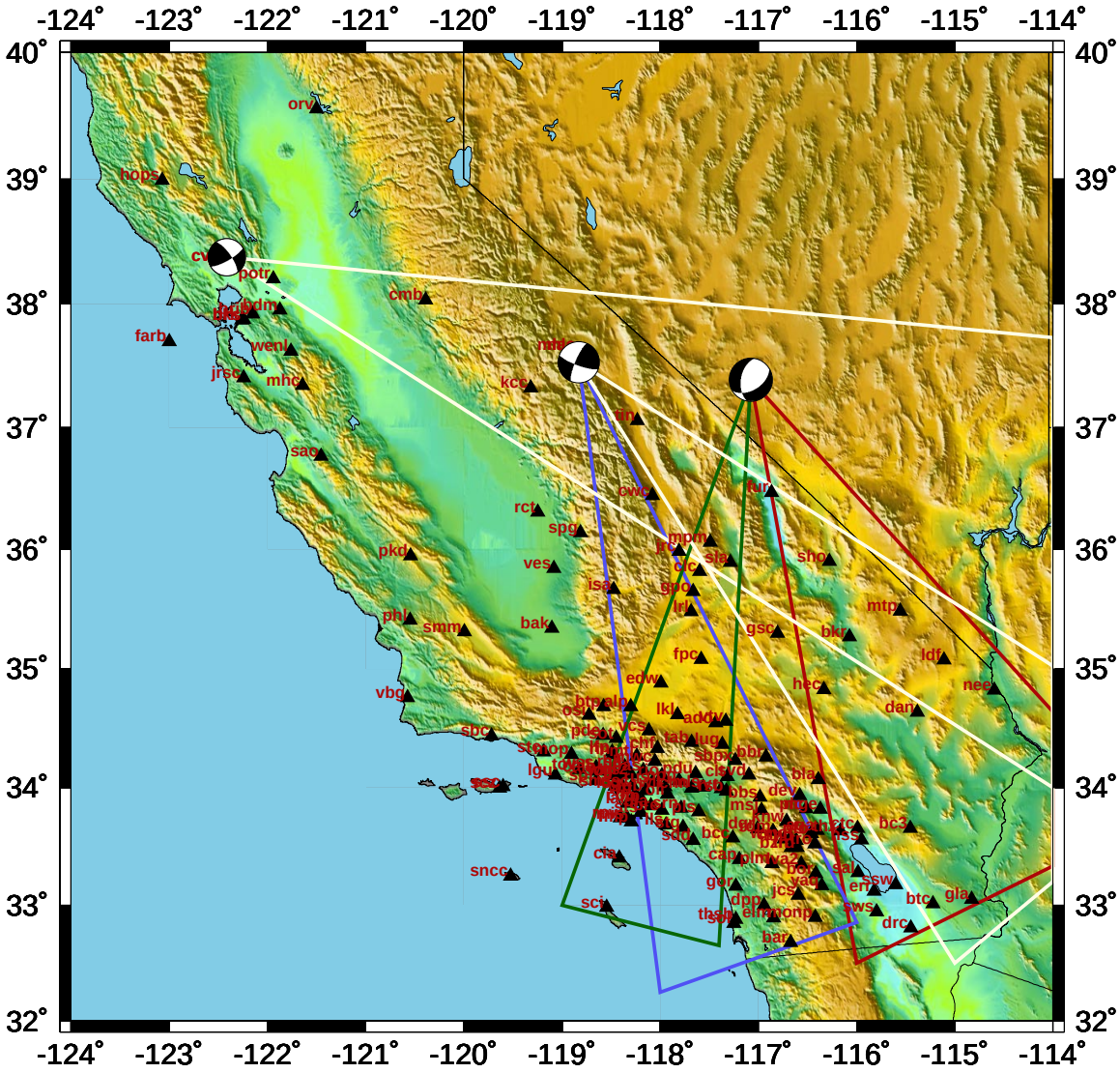

Figure 2. Map of California and Nevada, showing TriNet and BDSN stations as triangles, the focal mechanisms used for this study and the profiles modeled using Pnl waveforms

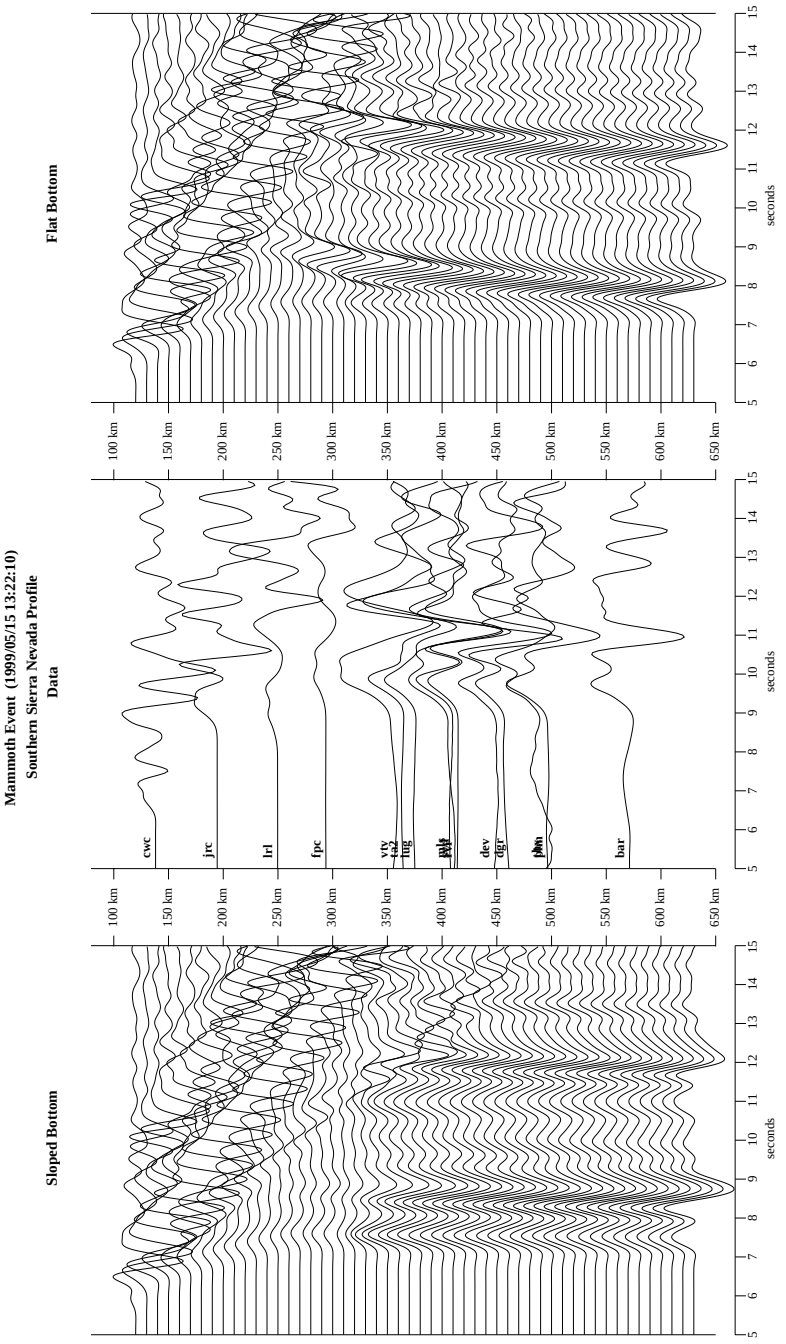

Figure 3. a) Synthetics created from the model in figure 5b with a sloped bottom b) Record section of the Mammoth event traversing the southern Sierra Nevada. The data is reduced using a velocity of 8.0 km/sec. The profile in map view is shown in figure 2 in blue. c) Velocity model synthetics with a flat bottomed bathtub anomaly just below the crust at 7.6 km/sec in figure 5a

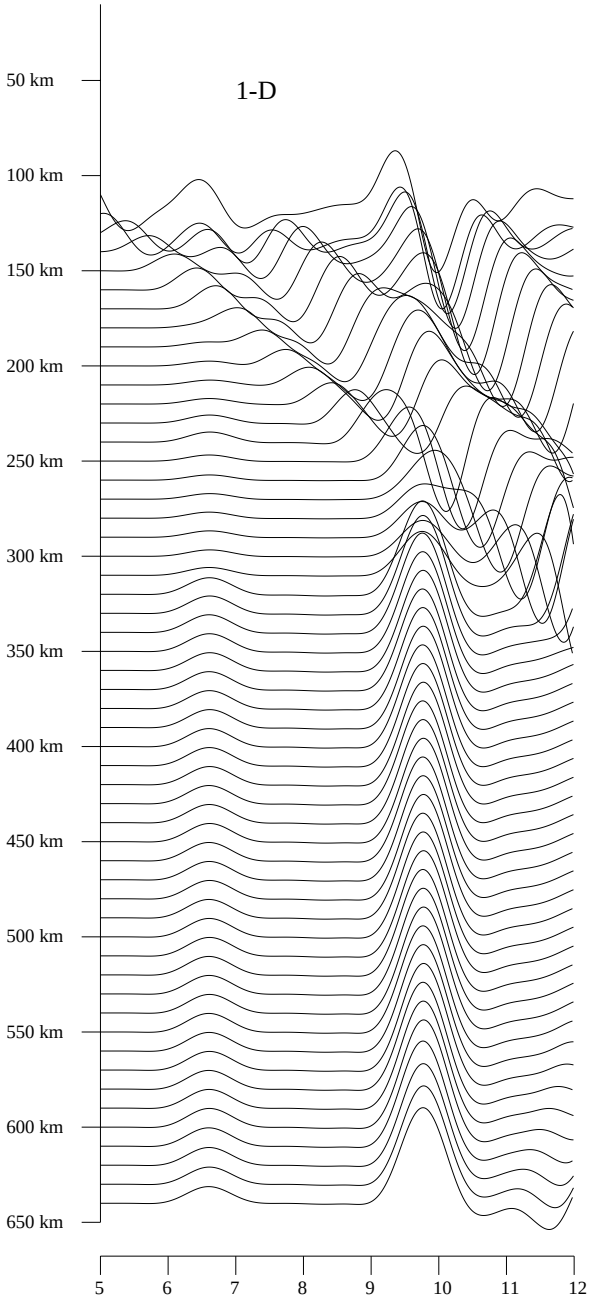

Figure 4. 1-D record section to indicate what Pn and sPn look like in a layer over a half-space.

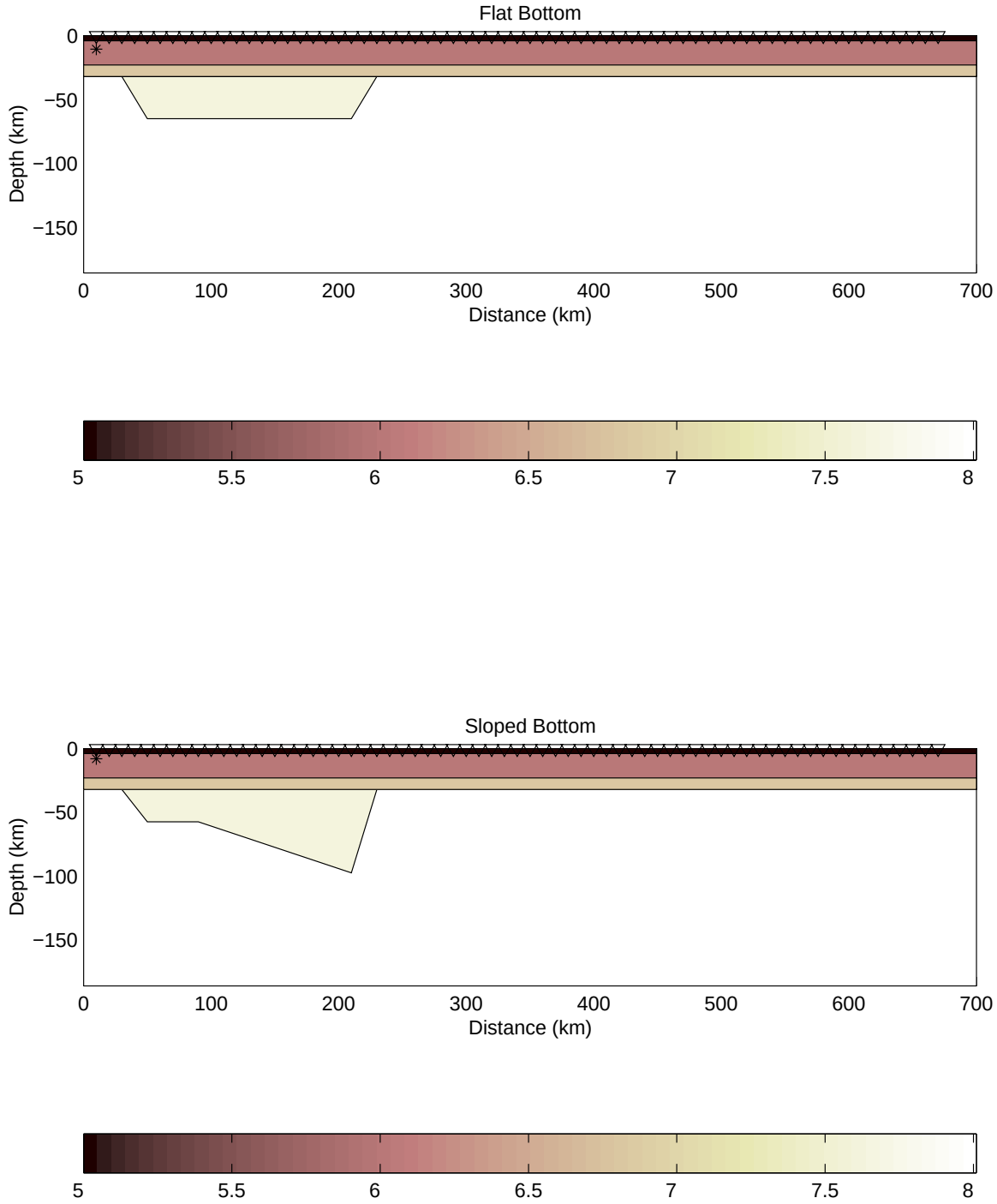

Figure 5. a) Velocity model with a flat bottomed bathtub anomaly just below the crust at 7.6 km/sec b) Model refinement of the model in a) by addition of a sloped bottom to align Pn and Pn?

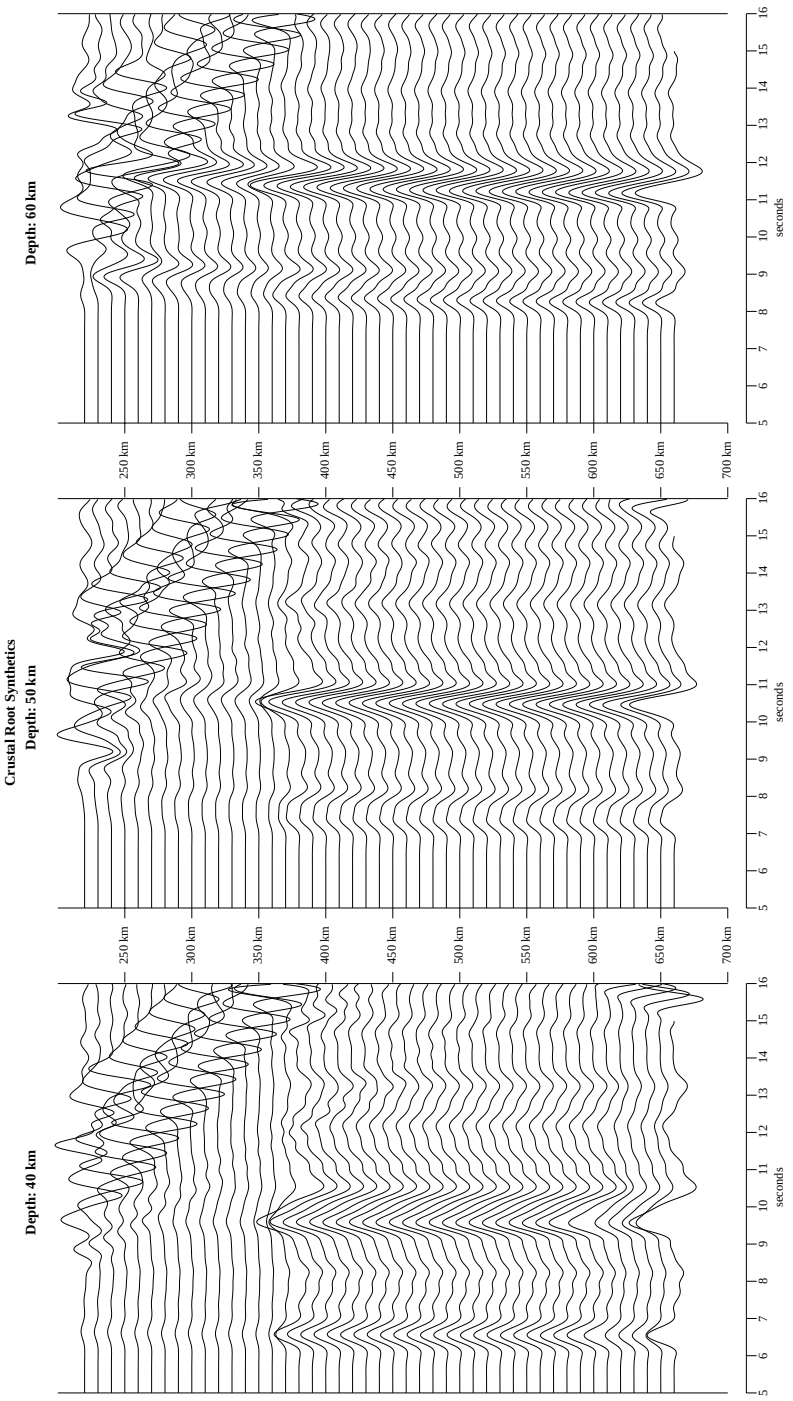

Figure 6. Synthetics for models with crustal roots from 40km to 60 km following Pakiser and Brune (1980)

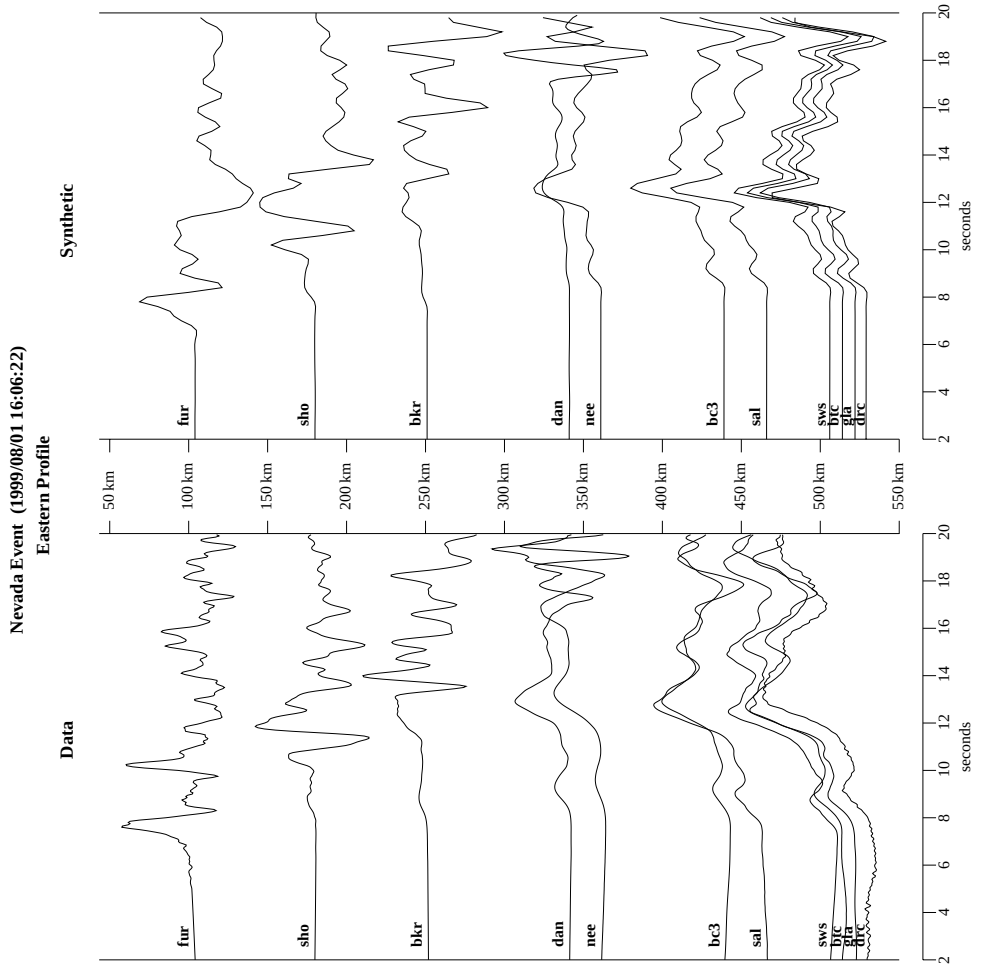

Figure 7. Comparison between data and synthetics for the eastern most profile marked in red in figure 2. The velocity depth section is shown in figure 8.

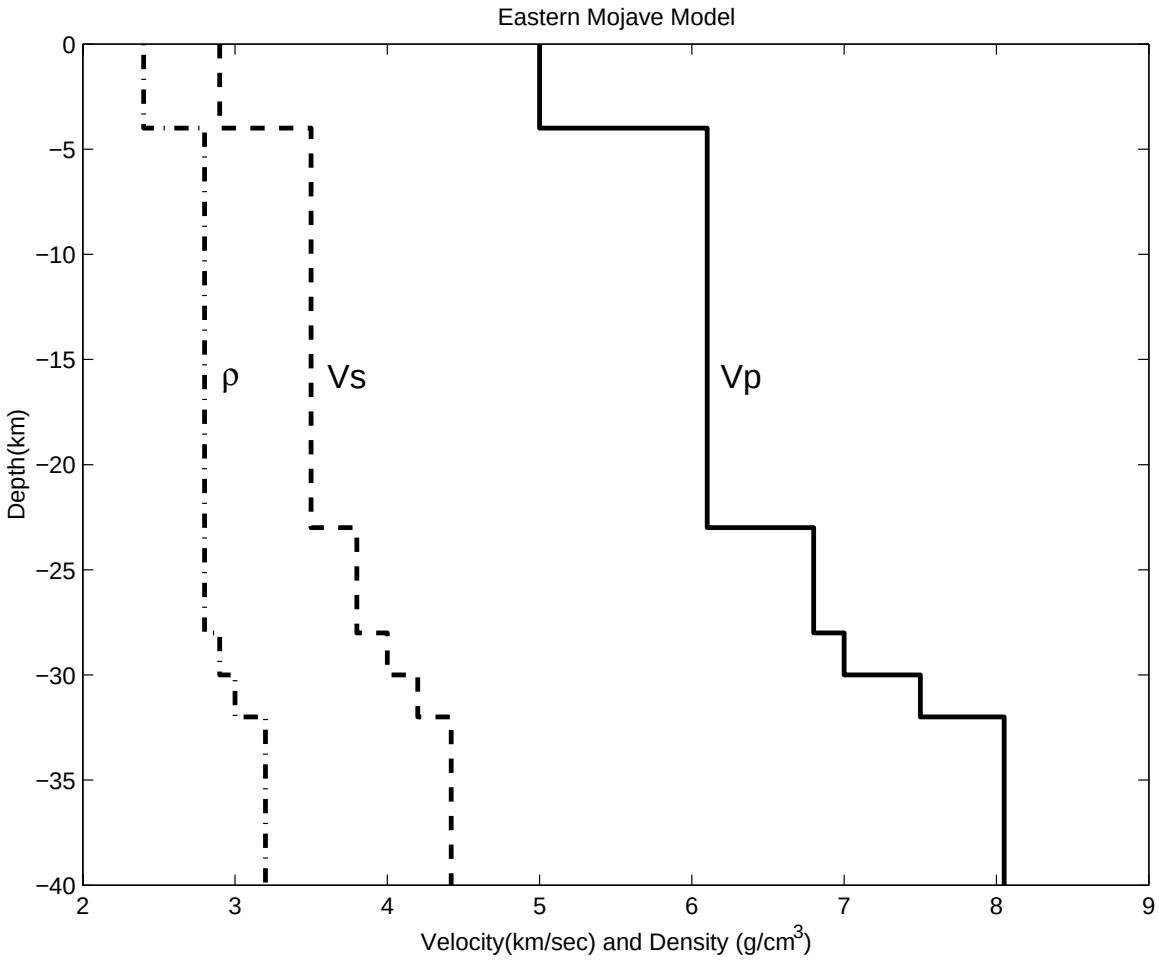

Figure 8. Depth velocity section of the eastern mojave model derived for the red section in figure 2.

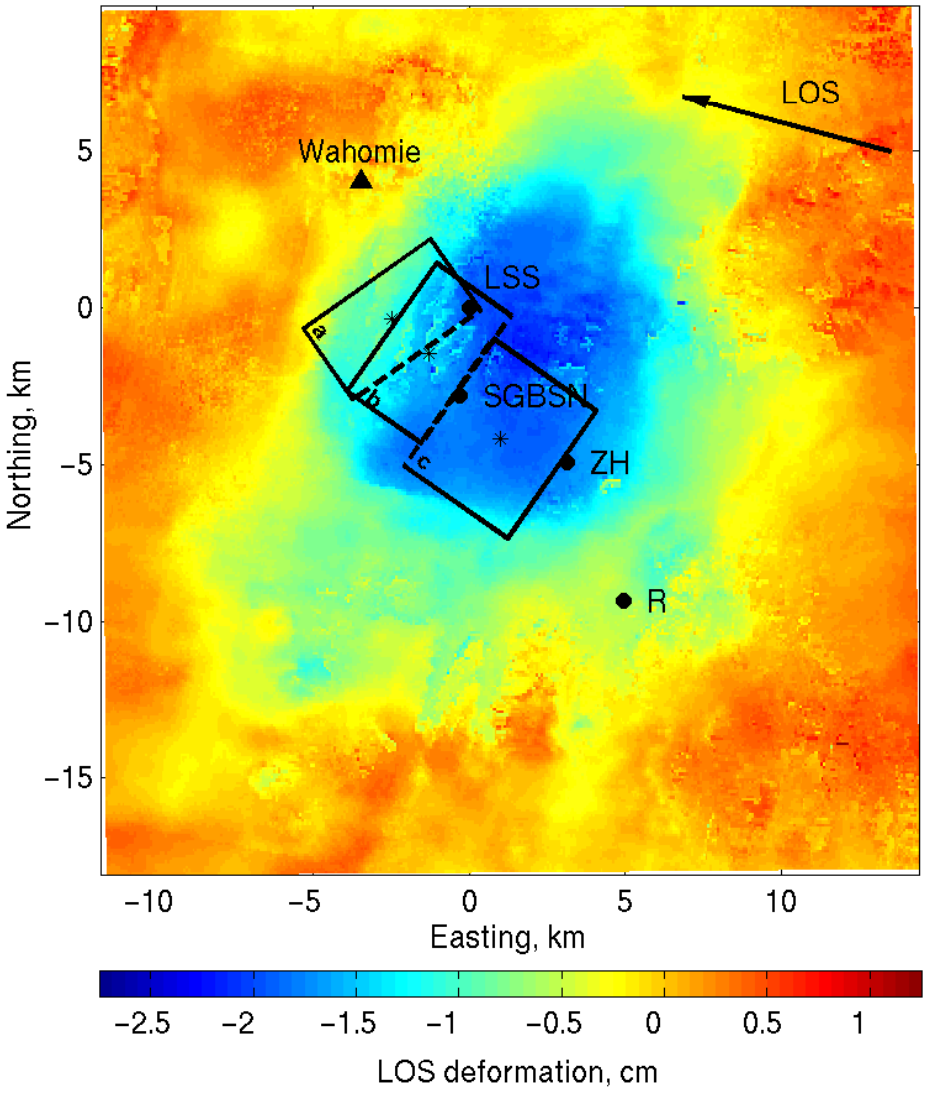

Figure 9. LOS displacement field from the averaged interferogram used in the inversions. The arrow indicates the surface projection of the LOS vector from the satellite to the ground. Note small-scale fluctuations due to tropospheric variations between scene acquisition dates. Geodetic benchmark Wahomie is shown as a filled triangle. LSM locations from Romanowicz et al., (1993) (R), Zhao and Helmberger, (1994) (ZH), and the SGBSN are indicated and labeled as is the best-fitting fault plane from our joint inversion (LSS) using the layered space from Jones and Helmberger, (1998). Rectangles show the fault planes used by (a) Savage et al., (1999), and the (b) SE-dipping and (c) NW-dipping planes in Wernicke et al., (1998). The dashed line indicates the bottom of the plane in all cases. This and all subsequent maps use a UTM (zone 11) projection. The origin (0,0) corresponds to the center of our best-fitting fault plane (LSS).

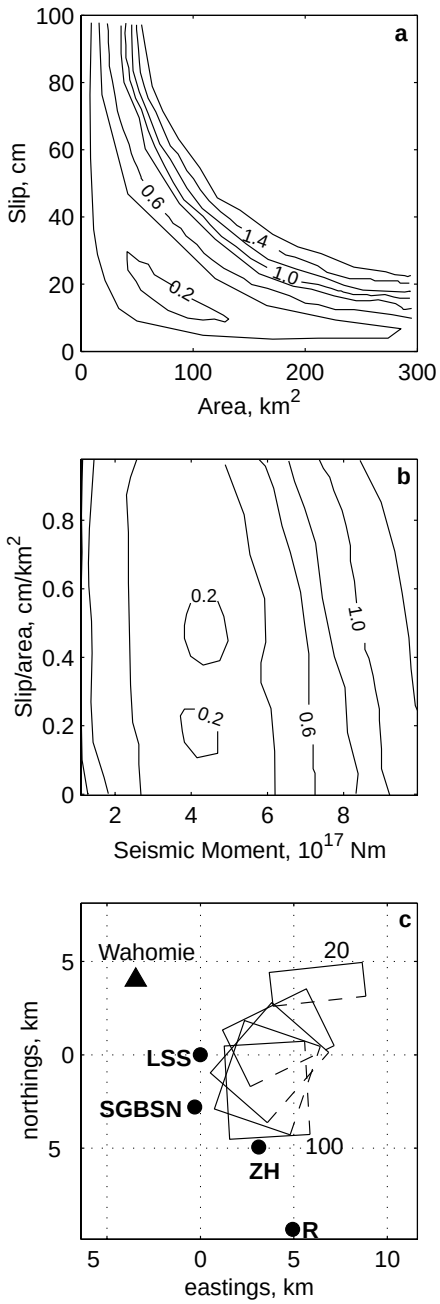

Figure 10. (a) Contours of RMS model misfit versus fault plane area and amount of slip. Misfit continues to increase to the upper right of the panel. (b) Contours of RMS model misfit versus moment and slip/area. Moment is calculated using μ=33 GPa. (c) Map view location of best-fitting planes with area 25 km^2 and rake fixed at values between -20^o and –100^o. Solid circles indicate the seismic locations of our best-fitting mechanism (LSS) from the joint inversion using the Mojave layered model, the Southern Great Basin Seismic Network (SGBSN), Zhao and Helmberger, (1994) (ZG), and Romanowicz et al., (1993) (R). All three panels correspond to inversions using only InSAR data and assume an elastic half space.

Figure 11. Mechanisms as well as observed waveforms and synthetic waveforms from the joint and InSAR-only inversions using the Mojave layered model. Pnl waveforms are filtered from 0.01-0.05~Hz, while full waveforms are filtered from 0.01-0.2~Hz. Data are shown as black lines and synthetics as gray lines. The time scale is shown at the base of each group of plots, with the 20~second bar referring to the Pnl waveforms and the 60~second bar referring to the full waveforms.